PROCEEDINGS A

royalsocietypublishing.org/journal/rspa

Research

Cite this article: Petromichelakis I, Kougioumtzoglou IA. 2020 Addressing the curse of dimensionality in stochastic dynamics: a Wiener path integral variational formulation with free boundaries. *Proc. R. Soc. A* **476**: 20200385.
https://doi.org/10.1098/rspa.2020.0385

Received: 15 May 2020
Accepted: 21 October 2020

Subject Areas:
applied mathematics, mechanics, mechanical engineering

Keywords:
high-dimensional systems, stochastic dynamics, path integral, variational formulation, dimension reduction, uncertainty quantification

Author for correspondence:
Ioannis A. Kougioumtzoglou
e-mail: ikougioum@columbia.edu

Addressing the curse of dimensionality in stochastic dynamics: a Wiener path integral variational formulation with free boundaries

Ioannis Petromichelakis and

Ioannis A. Kougioumtzoglou

Department of Civil Engineering and Engineering Mechanics, Columbia University, 500 W 120th Street, New York, NY 10027, USA

IP, 0000-0003-4916-7170

A Wiener path integral variational formulation with free boundaries is developed for determining the stochastic response of high-dimensional nonlinear dynamical systems in a computationally efficient manner. Specifically, a Wiener path integral representation of a marginal or lower-dimensional joint response probability density function is derived. Due to this *a priori* marginalization, the associated computational cost of the technique becomes independent of the degrees of freedom (d.f.) or stochastic dimensions of the system, and thus, the 'curse of dimensionality' in stochastic dynamics is circumvented. Two indicative numerical examples are considered for highlighting the capabilities of the technique. The first relates to marine engineering and pertains to a structure exposed to nonlinear flow-induced forces and subjected to non-white stochastic excitation. The second relates to nano-engineering and pertains to a 100-d.f. stochastically excited nonlinear dynamical system modelling the behaviour of large arrays of coupled nano-mechanical oscillators. Comparisons with pertinent Monte Carlo simulation data demonstrate the computational efficiency and accuracy of the developed technique.

1. Introduction

Ever-increasing computational capabilities, novel signal processing techniques, advanced experimental set-ups,

THE ROYAL SOCIETY PUBLISHING

as well as progress in emerging and transformative technologies (e.g. nano-mechanics) have contributed to a highly sophisticated mathematical modelling of the governing equations of diverse dynamical systems. In general, the governing dynamics is modelled as a high-dimensional system of coupled nonlinear (stochastic) differential equations. In many cases, solving even the deterministic version of such equations is an open issue and an active research topic. Clearly, addressing the stochastic counterparts of these equations becomes significantly more challenging, since the stochastic dimensions of the problem need to be considered in addition to the system deterministic/physical coordinates; thus, the overall dimensionality and computational complexity of the problem increase (e.g. [1]).

To address the above-described 'curse of dimensionality', as it is typically referred to in the relevant literature, researchers have developed diverse techniques for solving high-dimensional stochastic equations in a computationally efficient manner. Indicatively, these range from 'smart' Monte Carlo simulation (MCS) schemes (e.g. [2,3]) to various approximate dimension/order reduction approaches (e.g. [1]). Nevertheless, in most cases, these methodologies become eventually computationally prohibitive with an increasing number of problem dimensions.

Further, it can be argued that a complete stochastic characterization of the dynamical system response (i.e. determination of the joint response probability density function (PDF)) is not required for the vast majority of practical problems. Instead, determining a relatively small number of marginal PDFs, or low-dimensional joint PDFs, is often adequate in practice. In this regard, an interesting class of solution techniques focus on developing transformed governing stochastic equations involving only a subset of marginalized joint PDFs. The rationale relates to decreasing the dimensionality of the original problem and to determining directly the stochastic response of specific degrees of freedom (d.f.) or intrinsic coordinates of interest. Indicatively, appropriate multi-dimensional integration was applied in [4] for deriving PDF evolution equations corresponding to specific quantities of interest. Moreover, high-dimensional Fokker–Planck (F-P) equations were solved in [5] based on a block decomposition of the high-dimensional unobserved subset of variables and of the remaining low-dimensional observed variables. In a relatively similar context, a stochastic collocation scheme was developed in [6] capable of treating high-dimensional stochastic differential equations (SDEs) by constructing a sparse grid of collocation points, which is only weakly dependent on the dimensionality of the state space (see also [7]). Also, it is worth mentioning current research efforts based on deep learning tools for facilitating the solution of complex SDEs (e.g. [8]).

Herein, attention is directed to an alternative recently developed solution technique for stochastic engineering dynamics problems (e.g. [9–15]), which is based on the concept of the Wiener path integral (WPI) [16,17]. The technique, which relies on functional integration elements and resorts to a variational formulation, is capable of addressing a wide range of dynamical systems exhibiting diverse nonlinear/hysteretic behaviours [9,10], and subjected to non-white and non-Gaussian excitation stochastic processes [11]. Further, the technique can account also for fractional derivative terms in the governing equations [12], while it has been employed recently for stochastic analysis and optimization of a class of nonlinear electromechanical energy harvesters [13]. Furthermore, it is worth mentioning research efforts addressing not only stochastic dynamics problems with deterministic system parameters and stochastic excitations, but also a specific class of engineering mechanics problems with material parameters modelled as stochastic fields (e.g. [18]). Nevertheless, extending the WPI technique to account for general stochastic mechanics problems with media properties modelled as stochastic fields remains an open challenge.

Although the technique exhibits a relatively high degree of accuracy, its standard numerical implementation leads eventually to prohibitive computational cost with an increasing number of stochastic dimensions. This is due to the fact that the complete joint response PDF is determined by resorting to a point-wise computation on a multi-dimensional lattice. Clearly, this hinders the scalability of the technique in addressing multi-d.f. systems described by more than a few d.f.s. Although this limitation has been partly addressed in [14,15] by employing multi-dimensional function approximation techniques in conjunction with compressive sampling concepts and tools

for reducing the total number of grid-point calculations, the requirement for determining the complete joint response PDF has not been circumvented to date. Thus, the overall computational cost still grows rapidly with an increasing number of d.f.s.

In this paper, the curse of dimensionality in stochastic dynamics is addressed by marginalizing the joint response PDF based on a WPI variational formulation with free boundaries. In this regard, the associated computational cost becomes independent of the number of d.f.s; and thus, high-dimensional systems can be readily treated by the WPI technique. Two indicative numerical examples are considered for highlighting the capabilities of the technique. The first example relates to marine engineering and pertains to a structure exposed to nonlinear flow-induced forces and subjected to non-white stochastic excitation. The second example relates to nano-engineering and pertains to a 100-d.f. stochastically excited nonlinear dynamical system modelling the behaviour of large arrays of coupled nano-mechanical oscillators. Comparisons with pertinent MCS data demonstrate the computational efficiency and accuracy of the developed technique.

2. Preliminaries

(a) Governing stochastic equations

Consider a multi-dimensional first-order SDE of the general form

$$\mathrm{d}\boldsymbol{a} = \boldsymbol{A}\,(\boldsymbol{a},t)\,\mathrm{d}t + \boldsymbol{B}\,(\boldsymbol{a},t)\,\mathrm{d}\boldsymbol{W}, \tag{2.1}$$

where $\boldsymbol{W}$ represents a Wiener stochastic vector process with independent and normally distributed increments, and with continuous, but nowhere differentiable, sample paths (e.g. [19]). Under certain existence and uniqueness conditions related to (2.1) and assuming that $\boldsymbol{A}$ and $\boldsymbol{B}$ are continuous functions of t, $\boldsymbol{a}$ is a diffusion Markov stochastic vector process and $\tilde{\mathbf{B}}(\boldsymbol{a},t) := \boldsymbol{B}(\boldsymbol{a},t)\boldsymbol{B}^{\mathrm{T}}(\boldsymbol{a},t)$ denotes the diffusion matrix, which is symmetric and positive semidefinite. Notwithstanding some loss of mathematical rigour (e.g. [19]), (2.1) is ordinarily written, alternatively, as

$$\dot{\boldsymbol{a}} = \boldsymbol{A}\,(\boldsymbol{a},t) + \boldsymbol{B}\,(\boldsymbol{a},t)\,\boldsymbol{\eta}(t), \tag{2.2}$$

where $\boldsymbol{\eta}(t)$ is a zero-mean and delta-correlated process of intensity one, i.e. $\mathbb{E}[\boldsymbol{\eta}(t)] = \mathbf{0}$ and $\mathbb{E}[\boldsymbol{\eta}(t)\boldsymbol{\eta}^{\mathrm{T}}(t+\tau)] = \delta(\tau)\mathbf{I}$, where $\delta(t)$ is the Dirac delta function and $\mathbb{E}[.]$ denotes the expectation operator. Further, the solution of (2.2) can be expressed in the form of the joint transition PDF $p(\boldsymbol{a}_{i+1}, t_{i+1}|\boldsymbol{a}_i, t_i)$ satisfying the F-P equation (e.g. [20]).

In the ensuing analysis, a novel technique based on a WPI variational formulation with free boundaries is developed, which enables the marginalization of the joint PDF in an a priori manner. This significant advantage reduces, appropriately, the dimensionality of the original problem; and thus, renders the solution of (2.2) computationally tractable, even for high-dimensional systems.

(b) WPI and Lagrangian function

In this section, the salient aspects of the WPI formalism are presented for completeness. The interested reader is also directed to [16,17] for more details. Specifically, denoting $\Delta t = t_{i+1} - t_i$, considering $\Delta t \to 0$, and assuming a non-singular diffusion matrix $\tilde{\mathbf{B}}$, the transition PDF associated with the diffusion process $\boldsymbol{a}(t)$ of (2.2) has been shown to admit a Gaussian distribution (e.g. [20]) of the form

$$p(\boldsymbol{a}_{i+1}, t_{i+1}|\boldsymbol{a}_i, t_i) = \left[\sqrt{(2\pi\,\Delta t)^n \det\left[\tilde{\mathbf{B}}\,(\boldsymbol{a}_i, t_i)\right]}\right]^{-1}$$
$$\times \ldots \exp\left(-\frac{1}{2}\frac{\left[\boldsymbol{a}_{i+1} - \boldsymbol{a}_i - \Delta t\boldsymbol{A}\,(\boldsymbol{a}_i, t_i)\right]^{\mathrm{T}}\left[\tilde{\mathbf{B}}\,(\boldsymbol{a}_i, t_i)\right]^{-1}\left[\boldsymbol{a}_{i+1} - \boldsymbol{a}_i - \Delta t\boldsymbol{A}\,(\boldsymbol{a}_i, t_i)\right]}{\Delta t}\right). \tag{2.3}$$

Next, the probability that $\boldsymbol{a}(t)$ follows a specific path $\bar{\boldsymbol{a}}(t)$ can be expressed as the limiting case of the probability of the compound event

$$P[\bar{\boldsymbol{a}}(t)] = \lim_{\substack{\Delta t\to 0\\ N\to\infty}} P\left[\bigcap_{i=1}^{N}\left\{\boldsymbol{a}_i \in \left[\bar{\boldsymbol{a}}_i, \bar{\boldsymbol{a}}_i + [\mathrm{d}a_{ji}]_{n\times 1}\right]\right\}\right]$$
$$= \lim_{\substack{\Delta t\to 0\\ N\to\infty}} \left\{\prod_{i=1}^{N} p(\bar{\boldsymbol{a}}_{i+1}, t_{i+1}|\bar{\boldsymbol{a}}_i, t_i)\prod_{j=1}^{n}\mathrm{d}a_{ji}\right\}. \tag{2.4}$$

In (2.4), the time is discretized into N time points (slices) Δt apart, and $\mathrm{d}a_{ji}$ denotes the infinitesimal element along dimension j at time t_i. In this manner, (2.4) represents the probability of the process to propagate through the infinitesimally thin tube surrounding $\bar{\boldsymbol{a}}(t)$. Since $\Delta t \to 0$, (2.3) can be substituted into (2.4), and taking into account the Markovian property of $\boldsymbol{a}(t)$, the probability $P[\bar{\boldsymbol{a}}(t)]$ becomes

$$P[\bar{\boldsymbol{a}}(t)] = \lim_{\substack{\Delta t\to 0\\ N\to\infty}} \left\{\left[\prod_{i=1}^{N}\left(\left[\sqrt{(2\pi\,\Delta t)^n \det\left[\tilde{\mathbf{B}}(\bar{\boldsymbol{a}}_i, t_i)\right]}\right]^{-1}\prod_{j=1}^{n}\mathrm{d}a_{ji}\right)\right]\right.$$
$$\left.\times \ldots \exp\left(-\frac{1}{2}\sum_{i=1}^{N}\frac{\left[\bar{\boldsymbol{a}}_{i+1} - \bar{\boldsymbol{a}}_i - \Delta t\boldsymbol{A}(\bar{\boldsymbol{a}}_i, t_i)\right]^{\mathrm{T}}\left[\tilde{\mathbf{B}}(\bar{\boldsymbol{a}}_i, t_i)\right]^{-1}\left[\bar{\boldsymbol{a}}_{i+1} - \bar{\boldsymbol{a}}_i - \Delta t\boldsymbol{A}(\bar{\boldsymbol{a}}_i, t_i)\right]}{\Delta t}\right)\right\}, \tag{2.5}$$

which leads to

$$P[\bar{\boldsymbol{a}}(t)] = \exp\left(-\int_{t_0}^{t_f}\mathcal{L}(\bar{\boldsymbol{a}}, \dot{\bar{\boldsymbol{a}}})\mathrm{d}t\right)\prod_{t=t_0}^{t_f}\mathrm{d}\boldsymbol{a}(t), \tag{2.6}$$

where

$$\mathcal{L}(\boldsymbol{a}, \dot{\boldsymbol{a}}) = \frac{1}{2}\left[\dot{\boldsymbol{a}} - \boldsymbol{A}(\boldsymbol{a}, t)\right]^{\mathrm{T}}\left[\tilde{\mathbf{B}}(\boldsymbol{a}, t)\right]^{-1}\left[\dot{\boldsymbol{a}} - \boldsymbol{A}(\boldsymbol{a}, t)\right] \tag{2.7}$$

denotes the Lagrangian function and $\prod_{t=t_0}^{t_f}\mathrm{d}\boldsymbol{a}(t)$ is a functional measure given by

$$\prod_{t=t_0}^{t_f}\mathrm{d}\boldsymbol{a}(t) = \prod_{j=1}^{n}\prod_{t=t_0}^{t_f}\frac{\mathrm{d}a_j(t)}{\sqrt{2\pi\left(\det\left[\tilde{\mathbf{B}}(\bar{\boldsymbol{a}}, t)\right]\right)^{\frac{1}{n}}\mathrm{d}t}}. \tag{2.8}$$

The interested reader is also directed to [10,11] for more details. Further, the total probability that the process $\boldsymbol{a}$ starts from $\boldsymbol{a}_0$ at time t_0 and ends up at $\boldsymbol{a}_f$ at t_f takes the form of a functional integral, which 'sums up' the probabilities associated with each and every path that $\boldsymbol{a}$ can possibly follow (e.g. [16]). In this regard, denoting by $\mathcal{C}\{\boldsymbol{a}_0, t_0; \boldsymbol{a}_f, t_f\}$ the set of all paths with initial state $\boldsymbol{a}_0$ at time t_0 and final state $\boldsymbol{a}_f$ at time t_f, the transition PDF is expressed as a functional integral (or WPI) in the form

$$p(\boldsymbol{a}_f, t_f|\boldsymbol{a}_0, t_0) = \int_{\mathcal{C}\{\boldsymbol{a}_0, t_0; \boldsymbol{a}_f, t_f\}}\exp\left(-\int_{t_0}^{t_f}\mathcal{L}(\boldsymbol{a}, \dot{\boldsymbol{a}})\,\mathrm{d}t\right)\prod_{t=t_0}^{t_f}\mathrm{d}\boldsymbol{a}(t). \tag{2.9}$$

(c) Most probable path approximation

Considering the significant challenges related to evaluating (2.9) analytically or numerically, researchers have ordinarily resorted to the following approximate technique, also referred to in the path integral literature as semiclassical approximation (e.g. [16]). Specifically, note that the largest contribution to the functional integral of (2.9) comes from the trajectory $\bar{\boldsymbol{a}}(t)$ for which the

integral in the exponential (also known as stochastic action) becomes as small as possible (e.g. [16]). This leads to the variational problem

$$\text{minimize} \quad \int_{t_0}^{t_f} \mathcal{L}\,(\boldsymbol{a}, \dot{\boldsymbol{a}})\,\mathrm{d}t. \tag{2.10}$$

The trajectory $\bar{\boldsymbol{a}}(t)$ satisfying (2.10) is also known as the 'most probable path' and can be used in conjunction with (2.9) for determining approximately a specific point of the system response transition PDF, i.e.

$$p(\boldsymbol{a}_f, t_f|\boldsymbol{a}_0, t_0) \approx C\ \exp\left(-\int_{t_0}^{t_f} \mathcal{L}\,(\bar{\boldsymbol{a}}, \dot{\bar{\boldsymbol{a}}})\,\mathrm{d}t\right), \tag{2.11}$$

where C is a normalization constant. Clearly, the most probable path $\bar{\boldsymbol{a}}(t)$ is the extremal that minimizes the functional in (2.10). According to the fundamental theorem of calculus of variations [21], $\bar{\boldsymbol{a}}(t)$ can be evaluated by employing the necessary condition that the first variation of the functional vanishes. Considering fixed initial and final conditions at t_0 and t_f, respectively, this condition leads to a multivariate boundary value problem (BVP) of the form

$$\mathcal{L}_{a_i} - \frac{\mathrm{d}}{\mathrm{d}t}\mathcal{L}_{\dot{a}_i} = 0 \quad i = 1, \ldots, n \tag{2.12}$$

and

$$a_i(t_0) = a_{i,0}, \quad a_i(t_f) = a_{i,f} \quad i = 1, \ldots, n, \tag{2.13}$$

where $\mathcal{L}_{a_i}$ and $\mathcal{L}_{\dot{a}_i}$ denote the derivatives of the Lagrangian with respect to a_i and $\dot{a}_i$, respectively. (2.12) represents the Euler–Lagrange (E-L) equations and (2.13) relates to the fixed boundary conditions.

3. Proposed methodology

(a) Marginalized joint PDF WPI representation

It becomes clear that a brute-force determination of the n-dimensional response transition PDF via (2.11) requires point-wise calculations on a n-dimensional lattice. This leads to an exponential growth of the computational cost as a function of the number n of d.f.s. In other words, discretizing each dimension of vector $\boldsymbol{a}$ into N points, N^n BVPs of the form of (2.12) and (2.13) need to be solved numerically for evaluating the joint response PDF via (2.11).

To circumvent this limitation, a technique is developed in this paper, capable of determining marginalized joint response PDFs, i.e. PDFs that involve only a subset of the components of vector $\boldsymbol{a}$. In the ensuing analysis, a marginalized transition PDF is denoted as $p(\boldsymbol{u}, t_f|\boldsymbol{a}_0, t_0)$, where $\boldsymbol{u} = \{a_{i,f}|i \in U\}$ and U is an arbitrary subset $U \subseteq \{1, \ldots, n\}$ with cardinality $p = |U|$. Assuming fixed initial conditions at t_0, the herein developed technique is capable of determining any p-dimensional (marginalized) joint response transition PDF $p(\boldsymbol{u}) = p(\boldsymbol{u}, t_f|\boldsymbol{a}_0, t_0)$ directly, i.e. at a computational cost that is exponentially related to the dimension p of the target PDF only, and is essentially independent of the dimension n of the original system.

In this regard, the corresponding path integral representation of the transition PDF takes the form

$$p(\boldsymbol{u}, t_0|\boldsymbol{a}_0, t_0) = \int_{\mathcal{C}\{\boldsymbol{a}_0, t_0; \boldsymbol{u}, t_f\}} \exp\left(-\int_{t_0}^{t_f} \mathcal{L}\,(\boldsymbol{a}, \dot{\boldsymbol{a}})\,\mathrm{d}t\right) \prod_{t=t_0}^{t_f} \mathrm{d}\boldsymbol{a}(t), \tag{3.1}$$

where $\mathcal{C}\{\boldsymbol{a}_0, t_0; \boldsymbol{u}, t_f\}$ denotes the space of all possible paths with initial state $(\boldsymbol{a}_0, t_0)$ and final state $(\boldsymbol{u}, t_f)$. Note that the coordinates $a_{i,f}$ with $i \notin U$ are considered free.

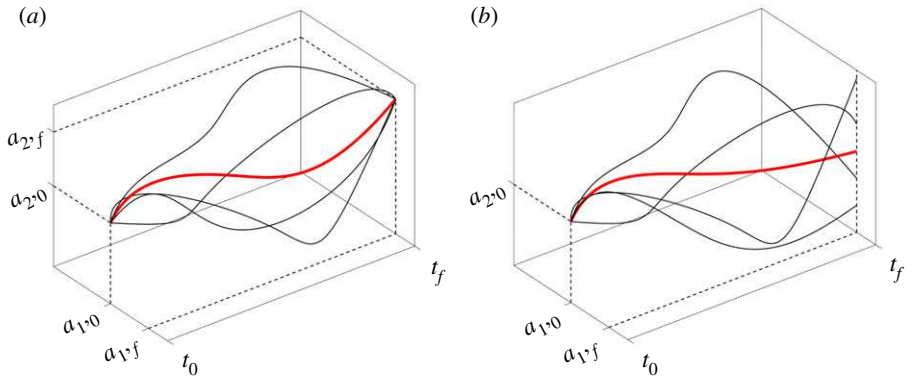

Figure 1. Indicative examples of sample paths (thin lines) and most probable path (thick line). (*a*) Fixed endpoint boundaries $a_{1,f}$ and $a_{2,f}$. (*b*) Fixed endpoint boundary $a_{1,f}$ and free endpoint boundary $a_{2,f}$. (Online version in colour.)

(b) Most probable path with free boundaries

Clearly, the most probable path, denoted as $\tilde{\boldsymbol{a}}(t)$ in the case of free endpoint boundaries, depends on the choice of set U, since this set determines which coordinates of $\tilde{\boldsymbol{a}}$ are fixed at the endpoint ($t = t_f$). Specifically, accounting for the free endpoint boundaries in the minimization of the functional in (2.10) leads to a BVP with the E-L equations of (2.12), but with the modified boundary conditions

$$a_i(t_0) = a_{i,0} \tag{3.2a}$$

$$\left.\begin{cases} a_i(t_f) = a_{i,f} & \text{if} \quad i \in U \\ \left[\mathcal{L}_{\dot{a}_i}\right]_{t=t_f} = 0 & \text{otherwise} \end{cases}\right\} \; i = 1, \ldots, n. \tag{3.2b}$$

Here (3.2*a*) represents the fixed initial conditions, whereas (3.2*b*) assigns a fixed endpoint condition to the components a_i of $\boldsymbol{a}$ with $i \in U$ and a free endpoint condition to the components a_i with $i \notin U$. The form of the free endpoint conditions in (3.2*a*) is the outcome of the first-order extremality condition with free endpoint boundaries (see appendix A for the complete derivation).

In this regard, a specific point of the marginalized system response transition PDF can be determined as

$$p(\boldsymbol{u}, t_f | \boldsymbol{a}_0, t_0) \approx C \, \exp\left(- \int_{t_0}^{t_f} \mathcal{L}\left(\tilde{\boldsymbol{a}}, \dot{\tilde{\boldsymbol{a}}}\right) \mathrm{d}t \right), \tag{3.3}$$

where C is a normalization constant. Indicative examples of sample paths and most probable paths corresponding both to (2.13) and (3.2) are shown in figure 1 for comparison.

(c) Generalization to higher-order SDEs

In this section, a generalization of the herein developed technique is presented, which accounts for higher-order systems of the form

$$\boldsymbol{x}^{(m)} = \boldsymbol{P}\left(\boldsymbol{x}, \ldots, \boldsymbol{x}^{(m-1)}, t\right) + \boldsymbol{Q}\left(\boldsymbol{x}, \ldots, \boldsymbol{x}^{(m-1)}, t\right) \boldsymbol{\eta}(t), \tag{3.4}$$

where $\boldsymbol{x}$ is a n-dimensional stochastic vector process, i.e. $\boldsymbol{x}(t) = [x_j(t)]_{n\times 1}$ and $\boldsymbol{x}^{(m)}$ denotes the mth-order derivative with respect to time t. Casting (3.4) into the form of (2.2), by setting $\boldsymbol{a} = [\boldsymbol{x}, \ldots, \boldsymbol{x}^{(m-1)}]^{\mathrm{T}}$, leads to a first-order system of nm SDEs characterized by a singular diffusion matrix $\tilde{\boldsymbol{B}}$. Thus, the Lagrangian in (2.7) cannot be used in a straightforward manner. However, it was shown in [11] that this type of diffusion matrix singularity can be treated effectively by

introducing delta functionals (i.e. the functional counterpart of the Dirac delta) into the path integral expression for enforcing the constraints $\dot{\boldsymbol{a}} = [\dot{\boldsymbol{x}}, \ldots, \boldsymbol{x}^{(m)}]^{\mathrm{T}}$. In this manner, functional integration of these delta functionals eliminates the variables corresponding to the singular part of $\tilde{\boldsymbol{B}}$. Ultimately, the path integral expression takes the form of (2.9) in conjunction, however, with a properly defined Lagrangian shown in (3.5) (see also [11]), i.e.

$$\mathcal{L}\left(\boldsymbol{x}, \ldots, \boldsymbol{x}^{(m)}\right) = \frac{1}{2}\left[\boldsymbol{x}^{(m)} - \boldsymbol{P}\left(\boldsymbol{x}, \ldots, \boldsymbol{x}^{(m-1)}, t\right)\right]^{\mathrm{T}} \left[\tilde{\mathbf{Q}}\left(\boldsymbol{x}, \ldots, \boldsymbol{x}^{(m-1)}, t\right)\right]^{-1} \times \left[\boldsymbol{x}^{(m)} - \boldsymbol{P}\left(\boldsymbol{x}, \ldots, \boldsymbol{x}^{(m-1)}, t\right)\right], \tag{3.5}$$

where

$$\tilde{\mathbf{Q}}\left(\boldsymbol{x}, \ldots, \boldsymbol{x}^{(m-1)}, t\right) = \mathbf{Q}\left(\boldsymbol{x}, \ldots, \boldsymbol{x}^{(m-1)}, t\right) \mathbf{Q}^{\mathrm{T}}\left(\boldsymbol{x}, \ldots, \boldsymbol{x}^{(m-1)}, t\right). \tag{3.6}$$

(d) Most probable path with free boundaries for higher-order SDEs

In a similar manner as in the first-order system of (2.2), the most probable path is determined as the trajectory that minimizes the functional $\int_{t_0}^{t_f} \mathcal{L}(\boldsymbol{x}, \ldots, \boldsymbol{x}^{(m)})\mathrm{d}t$ (see (2.10)). Assuming fixed initial and endpoint boundaries, the most probable path $\tilde{\boldsymbol{x}}(t)$ can be evaluated by solving the E-L equations

$$\sum_{k=0}^{m} (-1)^k \frac{\mathrm{d}^k}{\mathrm{d}t^k} \mathcal{L}_{x_i^{(k)}} = 0 \quad \text{for all} \quad i = 1, \ldots, n \tag{3.7}$$

together with the fixed boundary conditions. A specific point of the complete joint response transition PDF $p(\boldsymbol{x}_f, \ldots, \boldsymbol{x}_f^{(m-1)}, t_f | \boldsymbol{x}_0, \ldots, \boldsymbol{x}_0^{(m-1)}, t_0)$ can be obtained by using an expression similar to (2.11). On the other hand, a marginalized response transition PDF $p(\boldsymbol{u}, t_f | \boldsymbol{x}_0, \ldots, \boldsymbol{x}_0^{(m-1)}, t_0)$ can be determined by utilizing an expression of the form of (3.3). In this case, $\boldsymbol{u}$ denotes the p-dimensional vector that contains a prespecified number of endpoint coordinates, i.e. $1 \leq p \leq nm$ and $\boldsymbol{u} = \{x_{i,f}^{(k)} | i \in U_k\}$, where U_k is the set that contains the indices of the coordinates of the kth derivative $\boldsymbol{x}^{(k)}$ that participate in the marginalized PDF. For example, the marginal response PDF of the jth component of the rth derivative $x_j^{(r)}$ of $\boldsymbol{x}$ can be computed by setting $U_r = \{j\}$ and $U_k = \varnothing$ for all $k \neq r$. Next, accounting for the free endpoint boundaries in the minimization of the functional $\int_{t_0}^{t_f} \mathcal{L}(\boldsymbol{x}, \ldots, \boldsymbol{x}^{(m)})\mathrm{d}t$ leads to a BVP with the E-L equations of (3.7), but with the modified boundary conditions

$$x_i^{(k)}(t_0) = x_{i,0}^{(k)} \tag{3.8a}$$

$$\begin{cases} x_i^{(k)}(t_f) = x_{i,f}^{(k)} & \text{if} \quad i \in U_k \\ \left[\displaystyle\sum_{j=0}^{m-k-1} (-1)^j \frac{\mathrm{d}^j}{\mathrm{d}t^j} \mathcal{L}_{x_i^{(j+k+1)}}\right]_{t=t_f} = 0 & \text{otherwise.} \end{cases} \tag{3.8b}$$

These need to be considered for all $i = 1, \ldots, n$ and $k = 0, \ldots, m-1$, yielding a total number of $2mn$ boundary conditions. The solution of this problem provides the most probable path $\tilde{\boldsymbol{x}}(t)$, and a specific point of the marginalized response transition PDF is determined in the form

$$p(\boldsymbol{u}, t_f | \boldsymbol{x}_0, \ldots, \boldsymbol{x}_0^{(m-1)}, t_0) \approx C \exp\left(-\int_{t_0}^{t_f} \mathcal{L}\left(\tilde{\boldsymbol{x}}, \ldots, \tilde{\boldsymbol{x}}^{(m)}\right) \mathrm{d}t\right). \tag{3.9}$$

(e) Computational efficiency aspects

In the standard WPI solution technique (e.g. [11]), the complete nm-dimensional joint response PDF corresponding to the system of (3.4) is determined and marginalized by integration in an *a posteriori* manner. This procedure requires the discretization of the PDF effective domain into N^{nm} points, where N is the number of points along each dimension, and the response PDF at

a given time instant t_f is computed pointwise on the corresponding lattice. This leads to an exponential growth of the computational cost as a function of the dimensionality n and the order m of the system, since N^{nm} BVPs with fixed boundaries of the form of (2.12) and (2.13) need to be solved numerically. This limitation of the standard WPI technique has been partly addressed in [14,15] by employing multi-dimensional function approximation techniques in conjunction with compressive sampling concepts and tools for reducing the total number of required BVPs to be solved. However, notwithstanding the significant reduction of the associated computational cost achieved in [14,15], the requirement of the technique for determining the complete joint response PDF has not been circumvented to date. Clearly, this limits the scalability of the methodology since the number of BVPs to be solved becomes, eventually, prohibitive with an increasing number n of d.f.s.

By contrast, the technique developed in this paper is capable of determining any marginal p-dimensional response PDF by solving only N^p BVPs with free boundaries of the form of (3.8). This constitutes a reduction of the computational cost by orders of magnitude compared with the standard WPI technique. Notably, even in cases where the objective is to determine all marginal response PDFs of an n-dimensional system of mth order, the free boundaries WPI solution formalism requires a dramatically smaller number of BVPs to be solved than the fixed boundaries WPI formulation, i.e. $nmN \ll N^{mn}$. Clearly, in many practical problems where decision-making is based only on a readily identified most critical d.f., the computational efficiency enhancement becomes even more impressive, and the above relationship becomes $N \ll N^{mn}$. Obviously, selecting an optimal value of N for attaining a satisfactory compromise between accuracy and efficiency depends highly on the specific form of the nonlinear system under consideration. Nevertheless, based on various diverse numerical examples considered in [9–15] pertaining to engineering dynamics, it can be argued a value of N within the range $30 < N < 50$ constitutes a reasonable choice. Further, it is noted that the technique can be used in conjunction with the sparse representations approaches developed in [14,15], or following the determination of a reduced order system of governing equations based on various alternative dimensionality reduction methods. This is an additional significant advantage of the technique since the effect on reducing the overall computational cost is accumulative. Finally, indicative comparisons with a standard MCS-based solution approach can be found in the numerical examples of the following section.

4. Applications

In this section, the herein developed technique is used for determining marginalized joint response PDFs of various multi-d.f. nonlinear dynamical systems typically encountered in engineering applications. In general, a wide range of systems in stochastic engineering dynamics can be modelled as an n-d.f. system of the form

$$\mathbf{M}\ddot{\boldsymbol{x}} + \mathbf{C}\dot{\boldsymbol{x}} + \mathbf{K}\boldsymbol{x} + \boldsymbol{g}\,(\boldsymbol{x}, \dot{\boldsymbol{x}}, t) = \boldsymbol{D}\boldsymbol{\eta}(t), \tag{4.1}$$

where $\boldsymbol{x}(t) = [x_j(t)]_{n\times 1}$ is the displacement vector process; $\mathbf{M}$ is a $n \times n$ diagonal mass matrix; $\mathbf{C}$ and $\mathbf{K}$ are the $n \times n$ damping and stiffness matrices, respectively; $\boldsymbol{g}(\boldsymbol{x}, \dot{\boldsymbol{x}}, t) = [g_j(\boldsymbol{x}, \dot{\boldsymbol{x}}, t)]_{n\times 1}$ denotes an arbitrary nonlinear vector-valued function and $\mathbf{D}$ is a deterministic non-singular $n \times n$ matrix.

In the following, two distinct numerical examples are considered for demonstrating the reliability and computational efficiency of the developed WPI solution technique. Comparisons with pertinent MCS data, generated by utilizing a standard fourth-order Runge–Kutta scheme to numerically integrate the equations of motion, are included as well for assessing the accuracy of the technique.

The first example relates to marine engineering and pertains to a structure exposed to nonlinear flow-induced forces described by the Morison equation [22] and subjected to non-white

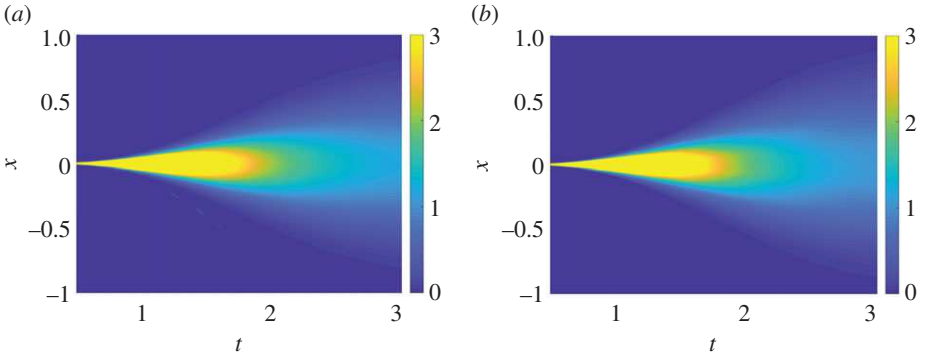

Figure 2. Evolution in time of the marginal response displacement PDF $p(x)$ pertaining to the Morison nonlinear system. (*a*) WPI. (*b*) MCS estimates (10 000 realizations). (Online version in colour.)

stochastic excitation. The second example relates to nano-engineering and pertains to a 100-d.f. stochastically excited nonlinear system modelling the behaviour of large arrays of coupled nanomechanical oscillators (e.g. [23–25]).

(a) Structural system subject to flow-induced forces

In this example, a single-d.f. oscillator under flow-induced forces is considered, typically modelled via the Morison nonlinear equation [22]. Further, the excitation is modelled as a non-white process compatible with the JONSWAP sea wave power spectrum, which is approximated herein by a second-order linear filter; see also [11] and references therein for more details. In this regard, the equations of motion become

$$\mu\ddot{y} + \gamma\dot{y} + \kappa y = w(t) \tag{4.2a}$$

and

$$\ddot{x} + 2\omega\xi\dot{x} + \omega^2 x + \frac{1}{2}\frac{C_D\rho D}{M_0}|V + \dot{x}|(V + \dot{x}) = y(t), \tag{4.2b}$$

where the parameter values $\mu = 1.8268$, $\gamma = 0.4418$, $\kappa = 3.0213$, $\omega = 1.2566$, $\xi = 0.02$, $C_D = 1$, $\rho D/M_0 = 1.136$ and $V = 0$ are used in the ensuing analysis. Next, following [11], (4.2*b*) is substituted into (4.2*a*) yielding a fourth-order nonlinear SDE of the form of (3.4) to be solved by the proposed WPI solution methodology. Clearly, from a practical perspective, the higher-order derivatives $x^{(3)}$ and $\ddot{x}$, appearing in the fourth-order SDE due to the filter (4.2*a*), do not offer any additional information or insight for analysing and eventually designing the structural system. Thus, the herein developed marginalized WPI formulation appears ideal for eliminating variables $x^{(3)}$ and $\ddot{x}$ from the response process vector. Specifically, applying the free boundaries WPI technique, the evolution in time of the marginal response displacement PDF is shown in figure 2. Comparing with pertinent MCS data demonstrates the accuracy of the developed methodology. It is noted that the evaluation of a marginal PDF at a specific time instant requires the solution of $N = 31$ BVPs, whereas using the standard fixed boundaries WPI requires the solution of $N^4 = 923\,521$ BVPs (since marginalization follows after the joint PDF has been obtained first). Also, for this particular example, MCS based on 10 000 realizations requires approximately 1 h of computation time, whereas a marginal PDF is determined via the proposed free boundaries WPI technique in approximately 10 s on the same computer.

(b) High-dimensional arrays of coupled nonlinear nano-mechanical oscillators

Due to their minuscule size and high sensitivity, micro- and nano-electromechanical systems (MEMS and NEMS) have been proposed recently for applications in signal processing, laser

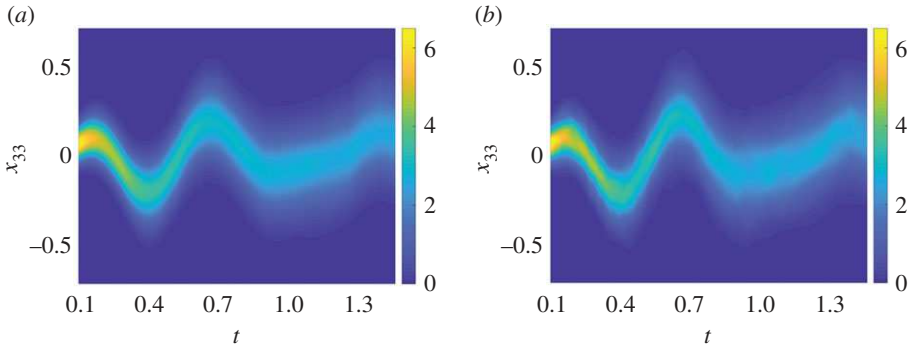

Figure 3. Evolution in time of the marginal response displacement PDF of x_{33}. (*a*) WPI. (*b*) MCS estimates (10 000 realizations). (Online version in colour.)

scanning, protein printing and label-free detection of molecules even in low concentrations [25]. In general, MEMS and NEMS can exhibit nonlinear response behaviour due to geometrical configurations and various damping mechanisms, are subject to various intrinsic sources of stochastic noise (e.g. adsorption–desorption and thermally induced noises), whereas, to enhance their detection sensitivity, current technology enables the fabrication of large arrays of nano-oscillators, coupled by electric, magnetic, or elastic forces [24,25]. In this regard, MEMS and NEMS are typically modelled as stochastically excited high-dimensional nonlinear multi-d.f. systems in the form of (4.1) [23,24]. Note, however, that due to the prohibitively large in many cases number of stochastic dimensions, the analysis of relatively large arrays of MEMS and NEMS has been performed to date based, primarily, on techniques that are subject to significant simplifications and approximations; see, for instance, [26] where a standard moments equations solution approach was employed, which is capable of providing relatively accurate estimates only for the system response first- and second-order statistics (e.g. mean and standard deviation); see also [27].

Next, the herein developed WPI technique is employed for determining marginalized joint response PDFs of a 100-d.f. MEMS modelled according to [24] and following (4.1) with

$$\mathbf{M}=\begin{bmatrix} m_0 & \cdots & 0 \\ \vdots & \ddots & \vdots \\ 0 & \cdots & m_0 \end{bmatrix} \quad \mathbf{C}=\begin{bmatrix} c_0 & \cdots & 0 \\ \vdots & \ddots & \vdots \\ 0 & \cdots & c_0 \end{bmatrix} \quad \mathbf{K}=\begin{bmatrix} k_0+2\omega_0 & -\omega_0 & \cdots & 0 \\ -\omega_0 & \ddots & \ddots & \vdots \\ \vdots & \ddots & \ddots & -\omega_0 \\ 0 & \cdots & -\omega_0 & k_0+2\omega_0 \end{bmatrix} \tag{4.3}$$

$$g(\boldsymbol{x},\dot{\boldsymbol{x}},t)=\left[\epsilon\left(\frac{x_j}{x_j^2+d_0^2}\right)^{3/2}-A\cos(\omega t)\right]_{100\times 1} \quad \mathbf{D}=\begin{bmatrix} \sqrt{10\pi} & \cdots & 0 \\ \vdots & \ddots & \vdots \\ 0 & \cdots & \sqrt{10\pi} \end{bmatrix}.$$

The parameter values are $m_0=1$, $c_0=1.5$, $k_0=120$, $\omega_0=70.2\pi$, $\epsilon=0.1$, $d_0=0.1$, $A=20$ and $\omega=3\pi$.

In figure 3, the evolution in time of the marginal response displacement PDF of x_{33} is shown, whereas in figure 4 the evolution in time of the joint response PDF $p(x_{97},\dot{x}_{97})$ is plotted. Comparisons with MCS data demonstrate the high degree of accuracy exhibited by the technique.

It is worth noting that in this example $N=31$ BVPs are solved for evaluating a marginal PDF at a specific time instant. Even in the case that knowledge of the marginal response displacement PDFs for all d.f.s is required, this translates into solving only $100\cdot 31=3100$ BVPs. By contrast, the standard WPI technique, which unavoidably determines the complete joint response PDF, requires the solution of 31^{200} BVPs, which is clearly a computationally intractable number.

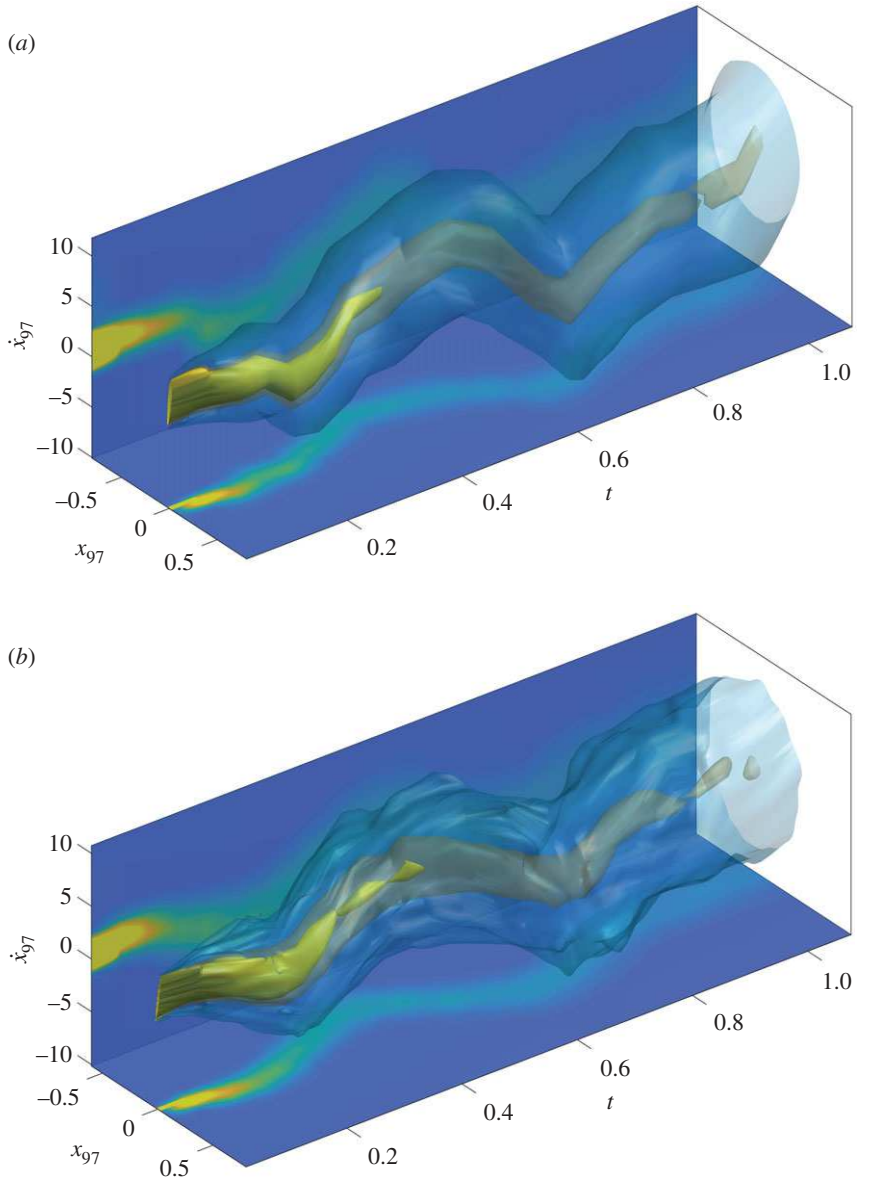

Figure 4. Evolution in time of the joint response PDF $p(x_{97}, \dot{x}_{97})$. (*a*) WPI and (*b*) MCS estimates (10 000 realizations). The three isosurfaces shown correspond to PDF values of 0.01 (blue), 0.32 (orange) and 0.6 (yellow). (Online version in colour.)

In figure 5, the accuracy and the efficiency of the proposed technique are compared with pertinent MCS results for a 10-d.f. version of the above nanomechanical oscillator at time $t = 0.5$ s. Specifically, the horizontal axis shows computational cost represented by actual computation time required based on a MATLAB_R2019a numerical implementation. The vertical axis shows the mean square error (MSE) between the estimated PDF and the target PDF based on MCS with 100 000 realizations (assumed to be exact for comparison purposes). The reported MSE corresponds to the average value accounting for all 20 marginal PDFs. In a similar manner, the computation time of the WPI shown on the horizontal axis corresponds to the average over the 20 marginal PDFs (i.e. 10 displacement and 10 velocity PDFs). MCS-based PDF estimates with a varying number of realizations are included as well. As anticipated, these estimates converge to

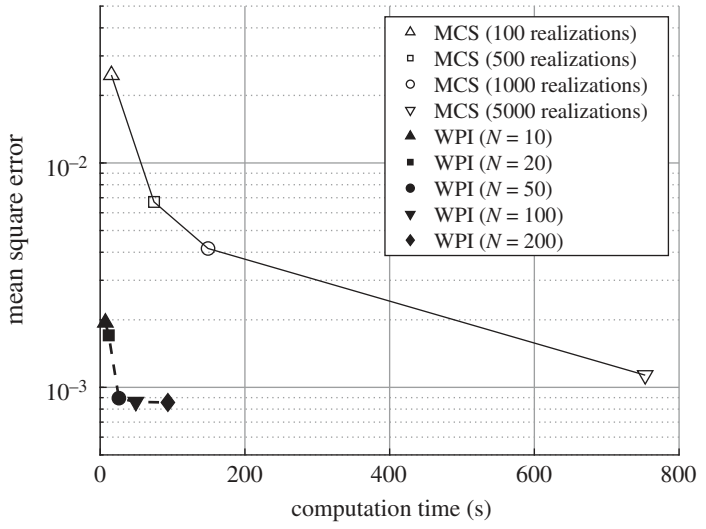

Figure 5. Comparisons between MCS and WPI technique in terms of accuracy and efficiency: mean square error and corresponding computation time for estimating a marginal PDF of a 10-d.f. nano-mechanical oscillator.

the target PDF with an increasing number of realizations, at the expense of course of increasing computational cost. Regarding the WPI-based PDF estimates, it is seen that the accuracy exhibited by the technique increases as the discretization of the PDF domain becomes finer. In other words, as the number N of BVPs to be solved becomes larger, the associated error becomes smaller. More importantly, in all cases, the performance of the WPI technique appears superior to that of the standard MCS. In fact, for approximately the same degree of accuracy, it is seen that the WPI-associated computation time is several orders of magnitude smaller than that corresponding to MCS.

5. Concluding remarks

A novel WPI variational formulation with free boundaries has been developed for determining the stochastic response of high-dimensional nonlinear dynamical systems in a computationally efficient manner. In this regard, the determination of the complete joint response PDF, required by the standard WPI implementation, has been circumvented herein by using a novel variational formulation involving free boundaries. The developed technique is capable of determining any lower-dimensional joint response PDF directly by properly selecting a combination of fixed and free boundaries at the end time point. Therefore, if knowledge of few only marginal or lower-dimensional joint response PDFs corresponding to a high-dimensional system is of interest, the technique constitutes a powerful tool that appears to be orders of magnitude more efficient than a standard MCS scheme.

Data accessibility. This article has no additional data.

Competing interests. We declare we have no competing interests.

Funding. I. A. Kougioumtzoglou gratefully acknowledges the support through his CAREER award by the CMMI Division of the National Science Foundation, USA (Award no. 1748537).

Acknowledgements. The authors would like to thank the anonymous reviewers for their constructive feedback that significantly enhanced the quality of the final paper.

A. Derivation of E-L equations and free-boundary conditions

Some basic variational calculus concepts are reviewed for completeness.

(a) First-order system of SDEs

The most probable path $\bar{\boldsymbol{a}}(t)$ corresponding to (2.2) is the function that minimizes the functional

$$S = \int_{t_0}^{t_f} \mathcal{L}\left(\boldsymbol{a}, \dot{\boldsymbol{a}}\right) \mathrm{d}t, \tag{A 1}$$

where the Lagrangian $\mathcal{L}$ is given in (2.7). Such a function is typically referred to as an *extremal* of functional S. According to the fundamental theorem of calculus of variations [21], an extremal can be evaluated by using the necessary condition that the first variation of the functional vanishes, i.e.

$$\delta S = 0 \tag{A 2}$$

in conjunction with appropriate boundary conditions. Assuming that the initial and final times t_0 and t_f are fixed, the first variation δS can be written as

$$\delta S = \int_{t_0}^{t_f} \left[\mathcal{L}\left(\boldsymbol{a} + \delta\boldsymbol{a}, \dot{\boldsymbol{a}} + \delta\dot{\boldsymbol{a}}\right) - \mathcal{L}\left(\boldsymbol{a}, \dot{\boldsymbol{a}}\right)\right] \mathrm{d}t, \tag{A 3}$$

where $\delta\boldsymbol{a}$ and $\delta\dot{\boldsymbol{a}}$ are the variations of functions $\boldsymbol{a}$ and $\dot{\boldsymbol{a}}$, respectively. By employing Taylor's formula, the first term of the integrand in (A 3) can be written as

$$\mathcal{L}\left(\boldsymbol{a} + \delta\boldsymbol{a}, \dot{\boldsymbol{a}} + \delta\dot{\boldsymbol{a}}\right) = \mathcal{L}\left(\boldsymbol{a}, \dot{\boldsymbol{a}}\right) + \sum_{i=1}^{n} \frac{\partial}{\partial a_i} \mathcal{L}\left(\boldsymbol{a}, \dot{\boldsymbol{a}}\right) \delta a_i + \sum_{i=1}^{n} \frac{\partial}{\partial \dot{a}_i} \mathcal{L}\left(\boldsymbol{a}, \dot{\boldsymbol{a}}\right) \delta \dot{a}_i + R, \tag{A 4}$$

where R is an infinitesimal of higher order than $\delta\boldsymbol{a}$ and $\delta\dot{\boldsymbol{a}}$. Next, combining equations (A 2)–(A 4), ignoring R and defining $\mathcal{L}_{a_i} = (\partial/\partial a_i)\mathcal{L}(\boldsymbol{a}, \dot{\boldsymbol{a}})$ and $\mathcal{L}_{\dot{a}_i} = (\partial/\partial \dot{a}_i)\mathcal{L}(\boldsymbol{a}, \dot{\boldsymbol{a}})$, the first variation of (A 3) takes the form

$$\begin{aligned} \delta S &= \int_{t_0}^{t_f} \sum_{i=1}^{n} \left[\mathcal{L}_{a_i} \delta a_i + \mathcal{L}_{\dot{a}_i} \delta \dot{a}_i\right] \mathrm{d}t \\ &= \sum_{i=1}^{n} \int_{t_0}^{t_f} \mathcal{L}_{a_i} \delta a_i \mathrm{d}t + \int_{t_0}^{t_f} \mathcal{L}_{\dot{a}_i} \delta \dot{a}_i \mathrm{d}t. \end{aligned} \tag{A 5}$$

Applying integration by parts on the second integral within the sum of (A 5) yields

$$\int_{t_0}^{t_f} \mathcal{L}_{\dot{a}_i} \delta \dot{a}_i \mathrm{d}t = \left[\mathcal{L}_{\dot{a}_i} \delta a_i\right]_{t_0}^{t_f} - \int_{t_0}^{t_f} \frac{\mathrm{d}}{\mathrm{d}t} \mathcal{L}_{\dot{a}_i} \delta a_i \mathrm{d}t. \tag{A 6}$$

Substituting (A 6) into (A 5), the necessary condition (i.e. (A 2)) for the minimization of functional S becomes

$$\delta S = \sum_{i=1}^{n} \left[\mathcal{L}_{\dot{a}_i} \delta a_i\right]_{t_0}^{t_f} + \sum_{i=1}^{n} \int_{t_0}^{t_f} \left(\mathcal{L}_{a_i} - \frac{\mathrm{d}}{\mathrm{d}t} \mathcal{L}_{\dot{a}_i}\right) \delta a_i \mathrm{d}t = 0. \tag{A 7}$$

(i) Fixed boundaries

Next, considering fixed initial and final conditions of the form

$$a_i(t_0) = a_{i,0} \quad \text{and} \quad a_i(t_f) = a_{i,f} \quad \text{for all} \quad i = 1, \ldots, n, \tag{A 8}$$

all variations δa_i vanish at the boundaries, i.e.

$$[\delta a_i]_{t=t_0} = [\delta a_i]_{t=t_f} = 0 \quad \text{for all} \quad i = 1, \ldots, n \tag{A 9}$$

and thus, (A 7) becomes

$$\sum_{i=1}^{n} \int_{t_0}^{t_f} \left(\mathcal{L}_{a_i} - \frac{\mathrm{d}}{\mathrm{d}t} \mathcal{L}_{\dot{a}_i}\right) \delta a_i \mathrm{d}t = 0. \tag{A 10}$$

Using the fundamental lemma of calculus of variations [28], leads to the well-known E-L equations of (2.12), which is a system of n coupled second-order ordinary differential

equations (ODEs) that can be solved together with the $2n$ boundary conditions of (2.13) for the determination of the most probable path $\bar{\boldsymbol{a}}(t)$.

(ii) Free boundaries

The problem of determining the most probable path $\tilde{\boldsymbol{a}}(t)$ is considered next, in which some of the endpoint boundaries are considered free. Thus, it is assumed that the initial conditions are fixed and that only a subset of the endpoint boundaries are fixed at $t = t_f$, i.e.

$$\left.\begin{aligned} a_i(t_0) &= a_{i,0} && \text{(A 11}a\text{)}\\ a_i(t_f) &= a_{i,f} \quad \text{if} \quad i \in U && \text{(A 11}b\text{)}\end{aligned}\right\} \; i = 1, \ldots, n,$$

whereas the rest $a_i(t_f)$ for which $i \notin U$ are considered free. It is noted that the set U, which determines what endpoint boundaries are fixed, is an arbitrary subset $U \subseteq \{1, \ldots, n\}$.

In this case, the variations at the boundaries take the form

$$\left.\begin{aligned} &[\delta a_i]_{t=t_0} = 0 && \text{(A 12}a\text{)}\\ &\begin{cases} [\delta a_i]_{t=t_f} = 0 & \text{if} \quad i \in U \\ [\delta a_i]_{t=t_f} = \delta a_{i,f} & \text{otherwise} \end{cases} && \text{(A 12}b\text{)}\end{aligned}\right\} \; i = 1, \ldots, n.$$

Note that $\tilde{\boldsymbol{a}}(t)$ is also an extremal with respect to the more restricted class of functions $\boldsymbol{a}(t)$ that have their boundaries fixed. Consequently, $\tilde{\boldsymbol{a}}(t)$ satisfies the E-L equation (2.12). In this regard, the second sum in (A 7) vanishes and taking (A 12) into account, (A 7) reduces to

$$\sum_{i \notin U} \left[\mathcal{L}_{\dot{a}_i} \delta a_i\right]_{t=t_f} = \sum_{i \notin U} \left[\mathcal{L}_{\dot{a}_i}\right]_{t=t_f} \delta a_{i,f} = 0. \tag{A 13}$$

Since the variations $\delta a_{i,f}$ are arbitrary, (A 13) leads to the additional boundary conditions $[\mathcal{L}_{\dot{a}_i}]_{t=t_f}$ for all $i \notin U$. Overall, the most probable path $\tilde{\boldsymbol{a}}(t)$ can be determined by solving the system of the n E-L equations in (2.12) together with the $2n$ modified boundary conditions of (3.2); see also [21,28] for a broader perspective.

(b) Higher-order system of SDEs

In this section, a generalization of the herein developed methodology is presented, which accounts for higher-order systems of the form of (3.4). The most probable path $\bar{\boldsymbol{x}}(t)$ corresponding to (3.4) is the function that minimizes the functional

$$S = \int_{t_0}^{t_f} \mathcal{L}\left(\boldsymbol{x}, \ldots, \boldsymbol{x}^{(m)}\right) \mathrm{d}t, \tag{A 14}$$

where $\mathcal{L}(\boldsymbol{x}, \ldots, \boldsymbol{x}^{(m)})$ is shown in (3.5).

Similarly as in the first-order case, $\bar{\boldsymbol{x}}(t)$ can be determined by considering the first-order extremality condition of (A 2). In the case of higher-order SDEs considered in this subsection, assuming that the initial and final times t_0 and t_f are fixed, the first variation δS takes the form

$$\delta S = \int_{t_0}^{t_f} \left[\mathcal{L}\left(\boldsymbol{x} + \delta\boldsymbol{x}, \ldots, \boldsymbol{x}^{(m)} + \delta\boldsymbol{x}^{(m)}\right) - \mathcal{L}\left(\boldsymbol{x}, \ldots, \boldsymbol{x}^{(m)}\right)\right] \mathrm{d}t, \tag{A 15}$$

where $\delta\boldsymbol{x},\ldots,\delta\boldsymbol{x}^{(m-1)}$ and $\delta\boldsymbol{x}^{(m)}$ are the variations of functions $\boldsymbol{x},\ldots,\boldsymbol{x}^{(m-1)}$ and $\boldsymbol{x}^{(m)}$, respectively. By employing Taylor's formula, the first term of the integrand in (A 15) can be written as

$$\begin{aligned}
&\mathcal{L}\left(\boldsymbol{x}+\delta\boldsymbol{x},\ldots,\boldsymbol{x}^{(m)}+\delta\boldsymbol{x}^{(m)}\right)\\
&\quad=\mathcal{L}\left(\boldsymbol{x},\ldots,\boldsymbol{x}^{(m)}\right)+\sum_{i=1}^{n}\frac{\partial}{\partial x_i}\mathcal{L}\left(\boldsymbol{x},\ldots,\boldsymbol{x}^{(m)}\right)\delta x_i+\sum_{i=1}^{n}\frac{\partial}{\partial \dot{x}_i}\mathcal{L}\left(\boldsymbol{x},\ldots,\boldsymbol{x}^{(m)}\right)\delta \dot{x}_i\\
&\qquad+\cdots\sum_{i=1}^{n}\frac{\partial}{\partial x_i^{(m)}}\mathcal{L}\left(\boldsymbol{x},\ldots,\boldsymbol{x}^{(m)}\right)\delta x_i^{(m)}+R\\
&\quad=\mathcal{L}\left(\boldsymbol{x},\ldots,\boldsymbol{x}^{(m)}\right)+\sum_{k=0}^{m}\sum_{i=1}^{n}\frac{\partial}{\partial x_i^{(k)}}\mathcal{L}\left(\boldsymbol{x},\ldots,\boldsymbol{x}^{(m)}\right)\delta x_i^{(k)}+R,
\end{aligned}\tag{A 16}$$

where R is an infinitesimal of higher order than $\delta\boldsymbol{x},\ldots,\delta\boldsymbol{x}^{(m-1)}$ and $\delta\boldsymbol{x}^{(m)}$. Next, combining equations (A 2), (A 15) and (A 16), ignoring R and defining $\mathcal{L}_{x_i^{(k)}}=(\partial/\partial x_i^{(k)})\mathcal{L}(\boldsymbol{x},\ldots,\boldsymbol{x}^{(m)})$, the first variation of (A 15) takes the form

$$\delta S=\sum_{k=0}^{m}\sum_{i=1}^{n}\int_{t_0}^{t_f}\mathcal{L}_{x_i^{(k)}}\delta x_i^{(k)}\mathrm{d}t.\tag{A 17}$$

Applying integration by parts once on the terms of (A 17) corresponding to $k=1$, twice on the terms corresponding to $k=2$, etc., yields

$$\begin{aligned}
&\int_{t_0}^{t_f}\mathcal{L}_{\dot{x}_i}\delta\dot{x}_i\,\mathrm{d}t=\left[\mathcal{L}_{\dot{x}_i}\delta x_i\right]_{t_0}^{t_f}-\int_{t_0}^{t_f}\frac{\mathrm{d}}{\mathrm{d}t}\mathcal{L}_{\dot{x}_i}\delta x_i\mathrm{d}t\\
&\int_{t_0}^{t_f}\mathcal{L}_{\ddot{x}_i}\delta\ddot{x}_i\,\mathrm{d}t=\left[\mathcal{L}_{\ddot{x}_i}\delta\dot{x}_i\right]_{t_0}^{t_f}-\left[\frac{\mathrm{d}}{\mathrm{d}t}\mathcal{L}_{\ddot{x}_i}\delta x_i\right]_{t_0}^{t_f}+\int_{t_0}^{t_f}\frac{i^2}{\mathrm{d}t^2}\mathcal{L}_{\ddot{x}_i}\delta x_i\mathrm{d}t\\
&\qquad\vdots\\
&\int_{t_0}^{t_f}\mathcal{L}_{x_i^{(m)}}\delta x_i^{(m)}\mathrm{d}t=\sum_{k=0}^{m-1}(-1)^k\left[\frac{i^{m-k-1}}{\mathrm{d}t^{m-k-1}}\mathcal{L}_{x_i^{(m)}}\delta x_i^{(k)}\right]_{t_0}^{t_f}+(-1)^m\int_{t_0}^{t_f}\frac{i^m}{\mathrm{d}t^m}\mathcal{L}_{x_i^{(m)}}\delta x_i\,\mathrm{d}t.
\end{aligned}\tag{A 18}$$

Substituting (A 18) into (A 17) and gathering terms of the same order k in variations $\delta x_i^{(k)}$, the necessary condition ((A 2)) for the minimization of functional S becomes

$$\begin{aligned}
\delta S&=\sum_{i=1}^{n}\left\{\left[\left(\sum_{k=0}^{m-1}(-1)^k\frac{i^k}{\mathrm{d}t^k}\mathcal{L}_{x_i^{(k+1)}}\right)\delta x_i\right]_{t_0}^{t_f}+\left[\left(\sum_{k=0}^{m-2}(-1)^k\frac{i^k}{\mathrm{d}t^k}\mathcal{L}_{x_i^{(k+2)}}\right)\delta\dot{x}_i\right]_{t_0}^{t_f}\right.\\
&\quad\left.+\cdots+\left[\mathcal{L}_{x_i^{(m)}}\delta x_i^{(m-1)}\right]_{t_0}^{t_f}+\int_{t_0}^{t_f}\left(\sum_{k=0}^{m}(-1)^k\frac{i^k}{\mathrm{d}t^k}\mathcal{L}_{x_i^{(k)}}\right)\delta x_i\mathrm{d}t\right\}\\
&=\sum_{i=1}^{n}\left\{\sum_{l=0}^{m-1}\left[\left(\sum_{k=0}^{m-l-1}(-1)^k\frac{i^k}{\mathrm{d}t^k}\mathcal{L}_{x_i^{(k+l+1)}}\right)\delta x_i^{(l)}\right]_{t_0}^{t_f}\right\}\\
&\quad+\sum_{i=1}^{n}\int_{t_0}^{t_f}\left(\sum_{k=0}^{m}(-1)^k\frac{i^k}{\mathrm{d}t^k}\mathcal{L}_{x_i^{(k)}}\right)\delta x_i\mathrm{d}t=0.
\end{aligned}\tag{A 19}$$

(i) Fixed boundaries

Next, considering fixed initial and final conditions of the form

$$x_i^{(k)}(t_0) = x_{i,0}^{(k)} \quad \text{and} \quad x_i^{(k)}(t_f) = x_{i,f}^{(k)} \quad \text{for all} \quad i = 1, \ldots, n \quad \text{and} \quad k = 0, \ldots, m-1, \tag{A 20}$$

all variations $\delta x_i^{(k)}$ vanish at the boundaries, i.e.,

$$\left[\delta x_i^{(k)}\right]_{t=t_0} = \left[\delta x_i^{(k)}\right]_{t=t_f} = 0 \quad \text{for all} \quad i = 1, \ldots, n \quad \text{and} \quad k = 0, \ldots, m-1 \tag{A 21}$$

and thus, (A 19) becomes

$$\sum_{i=1}^{n} \int_{t_0}^{t_f} \left(\sum_{k=0}^{m} (-1)^k \frac{\mathrm{d}^k}{\mathrm{d}t^k} \mathcal{L}_{x_i^{(k)}} \right) \delta x_i \mathrm{d}t = 0. \tag{A 22}$$

Utilizing the fundamental lemma of calculus of variations [28], leads to the E-L equations shown in (3.7), which is a system of n coupled $2m$th-order ODEs that can be solved together with the $2nm$ boundary conditions of (A 20) for the determination of the most probable path $\bar{\boldsymbol{x}}(t)$.

(ii) Free boundaries

The problem of determining the most probable path $\tilde{\boldsymbol{x}}(t)$ is considered next, in which some of the endpoint boundaries are considered free. Thus, it is assumed that the initial conditions are fixed and that only a subset of the endpoint boundaries are fixed at $t = t_f$, i.e.

$$\left.\begin{aligned} x_i^{(k)}(t_0) &= x_{i,0}^{(k)} && \text{(A 23a)} \\ x_i^{(k)}(t_f) &= x_{i,f}^{(k)} \quad \text{if} \quad i \in U_k && \text{(A 23b)} \end{aligned}\right\} \; i = 1, \ldots, n \quad \text{and} \quad k = 0, \ldots, m-1,$$

whereas the rest $x_i^{(k)}(t_f)$ for which $i \notin U_k$ are considered free. It is noted that the sets U_k, which determine what endpoint boundaries of kth-order are fixed, are arbitrary subset $U_k \subseteq \{1, \ldots, n\}$ for all $k = 0, \ldots, m-1$.

In this case, the variations at the boundaries take the form

$$\left.\begin{aligned} &\left[\delta x_i^{(k)}\right]_{t=t_0} = 0 && \text{(A 24a)} \\ &\begin{cases} \left[\delta x_i^{(k)}\right]_{t=t_f} = 0 & \text{if} \quad i \in U_k \\ \left[\delta x_i^{(k)}\right]_{t=t_f} = \delta x_{i,f}^{(k)} & \text{otherwise} \end{cases} && \text{(A 24b)} \end{aligned}\right\} \; i = 1, \ldots, n \quad \text{and} \quad k = 0, \ldots, m-1.$$

Note that $\tilde{\boldsymbol{x}}(t)$ is also an extremal with respect to the more restricted class of functions $\boldsymbol{x}(t)$ that have their boundaries fixed. Consequently, $\tilde{\boldsymbol{x}}(t)$ satisfies the E-L equation (3.7). In this regard, the corresponding sum in (A 19) vanishes and taking (A 24) into account, the remaining terms of (A 19) yield a set of boundary conditions corresponding to the free boundaries, i.e. the components $x_i^{(k)}$ for which $i \notin U_k$. The complete set of boundary conditions, considering a combination of fixed and free conditions, is shown in (3.8). Concisely, the most probable path $\tilde{\boldsymbol{x}}(t)$ can be determined by solving the system of the n E-L equations in (3.7) together with the 2 nm modified boundary conditions of (3.8).

References

1. Grigoriu M. 2012 *Stochastic systems: uncertainty quantification and propagation*. Berlin, Germany: Springer Science & Business Media.
2. Doucet A, De Freitas N, Gordon N. 2001 *An introduction to sequential Monte Carlo methods*. Berlin, Germany: Springer.
3. Au SK, Wang Y. 2014 *Engineering risk assessment with subset simulation*. New York, NY: John Wiley & Sons.

4. Venturi D, Karniadakis GE. 2014 Convolutionless Nakajima–Zwanzig equations for stochastic analysis in nonlinear dynamical systems. *Proc. R. Soc. A: Math. Phys. Eng. Sci.* **470**, 20130754. (doi:10.1098/rspa.2013.0754)
5. Chen N, Majda AJ. 2017 Beating the curse of dimension with accurate statistics for the Fokker–Planck equation in complex turbulent systems. *Proc. Natl Acad. Sci. USA* **114**, 12 864–12 869. (doi:10.1073/pnas.1717017114)
6. Xiu D, Hesthaven JS. 2005 High-order collocation methods for differential equations with random inputs. *SIAM J. Sci. Comput.* **27**, 1118–1139. (doi:10.1137/040615201)
7. Ma X, Zabaras N. 2010 An adaptive high-dimensional stochastic model representation technique for the solution of stochastic partial differential equations. *J. Comput. Phys.* **229**, 3884–3915. (doi:10.1016/j.jcp.2010.01.033)
8. Beck C, Weinan E, Jentzen A. 2019 Machine learning approximation algorithms for high-dimensional fully nonlinear partial differential equations and second-order backward stochastic differential equations. *J. Nonlinear Sci.* **29**, 1563–1619. (doi:10.1007/s00332-018-9525-3)
9. Kougioumtzoglou IA, Spanos PD. 2012 An analytical Wiener path integral technique for non-stationary response determination of nonlinear oscillators. *Probab. Eng. Mech.* **28**, 125–131. (doi:10.1016/j.probengmech.2011.08.022)
10. Petromichelakis I, Psaros AF, Kougioumtzoglou IA. 2020 Stochastic response determination of nonlinear structural systems with singular diffusion matrices: A Wiener path integral variational formulation with constraints. *Probab. Eng. Mech.* **60**, 103044. (doi:10.1016/j.probengmech.2020.103044)
11. Psaros AF, Brudastova O, Malara G, Kougioumtzoglou IA. 2018 Wiener Path Integral based response determination of nonlinear systems subject to non-white, non-Gaussian, and non-stationary stochastic excitation. *J. Sound Vib.* **433**, 314–333. (doi:10.1016/j.jsv.2018.07.013)
12. Di Matteo A, Kougioumtzoglou IA, Pirrotta A, Spanos PD, Di Paola M. 2014 Stochastic response determination of nonlinear oscillators with fractional derivatives elements via the Wiener path integral. *Probab. Eng. Mech.* **38**, 127–135. (doi:10.1016/j.probengmech.2014.07.001)
13. Petromichelakis I, Psaros AF, Kougioumtzoglou IA. 2018 Stochastic response determination and optimization of a class of nonlinear electromechanical energy harvesters: a Wiener path integral approach. *Probab. Eng. Mech.* **53**, 116–125. (doi:10.1016/j.probengmech.2018.06.004)
14. Psaros AF, Kougioumtzoglou IA, Petromichelakis I. 2018 Sparse representations and compressive sampling for enhancing the computational efficiency of the Wiener path integral technique. *Mech. Syst. Signal Process.* **111**, 87–101. (doi:10.1016/j.ymssp.2018.03.056)
15. Psaros AF, Petromichelakis I, Kougioumtzoglou IA. 2019 Wiener path integrals and multi-dimensional global bases for non-stationary stochastic response determination of structural systems. *Mech. Syst. Signal Process.* **128**, 551–571. (doi:10.1016/j.ymssp.2019.04.014)
16. Chaichian M, Demichev A. 2001 *Path integrals in physics: stochastic processes and quantum mechanics*. Bristol, UK: Institute of Physics Publishing.
17. Wio HS. 2013 *Path integrals for stochastic processes: an introduction*. Singapore: World Scientific Pub Co Inc.
18. Kougioumtzoglou IA. 2017 A Wiener path integral solution treatment and effective material properties of a class of one-dimensional stochastic mechanics problems. *J. Eng. Mech.* **143**, 04017014. (doi:10.1061/(ASCE)EM.1943-7889.0001211)
19. Gardiner CW. 2004 *Handbook of stochastic methods for physics, chemistry and the natural sciences*. Springer Series in Synergetics, 3rd edn. Berlin, Germany: Springer.
20. Risken H. 1996 *The Fokker–Planck equation: methods of solution and applications*. Berlin, Germany: Springer.
21. Gelfand IM, Fomin SV, Silverman RA. 2000 *Calculus of variations*. North Chelmsford, MA: Courier Corporation.
22. Morison JR, O'Brien MP, Johnson JW, Schaaf SA. 1950 The force exerted by surface waves on piles. *J. Petroleum Technol.* **2**, 149–154. (doi:10.2118/950149-G)
23. Perkins E, Kimura M, Hikihara T, Balachandran B. 2016 Effects of noise on symmetric intrinsic localized modes. *Nonlinear Dyn.* **85**, 333–341. (doi:10.1007/s11071-016-2688-2)
24. Lifshitz R, Cross MC. 2003 Response of parametrically driven nonlinear coupled oscillators with application to micromechanical and nanomechanical resonator arrays. *Phys. Rev. B* **67**, 134302. (doi:10.1103/PhysRevB.67.134302)

25. Eom K, Park HS, Yoon DS, Kwon T. 2011 Nanomechanical resonators and their applications in biological/chemical detection: nanomechanics principles. *Phys. Rep.* **503**, 115–163. (doi:10.1016/j.physrep.2011.03.002)
26. Ramakrishnan S, Balachandran B. 2010 Energy localization and white noise-induced enhancement of response in a micro-scale oscillator array. *Nonlinear Dyn.* **62**, 1–16. (doi:10.1007/s11071-010-9694-6)
27. Roberts JB, Spanos PD. 2003 *Random vibration and statistical linearization*. Mineola, NY: Dover Publications.
28. Elsgolc LD. 2007 *Calculus of variations*. Mineola, NY: Dover Publications.